Synthesis of Cast Magnesium Alloy (AZ91) Gr Composites by Bubbling Carbon Dioxide

Mehran Zare
Omid Ghaderi
Kaustubh Kishore Rane
Swaroop Kumar Behera
Department of Materials Science and Engineering, University of Wisconsin – Milwaukee, Milwaukee, Wisconsin, USA

Behzad Niroumand
Department of Materials Science and Engineering, Isfahan University of Technology, Isfahan, Iran

Pradeep K Rohatgi
Department of Materials Science and Engineering, University of Wisconsin – Milwaukee, Milwaukee, Wisconsin, USA

ABSTRACT

Magnesium (Mg) is considered an attractive lightweight metal due to its outstanding properties. However, Mg alloys are limited by their hexagonal closed-packed (HCP) structure and limited number of slip systems at room temperature. These disadvantages have driven researchers to develop Mg composites using various methods. Carbon dioxide (CO_2) injection is among the most advanced and environmentally friendly methods for synthesizing in-situ graphene (Gr) within molten metal. This paper reviews Gr-reinforced MMCs with a focus on Mg matrix composites, the mechanism of Gr formation within the Mg melt, and the impact of Gr on the mechanical properties of Mg alloys. Additionally, this paper presents recent developments from work conducted at the University of Wisconsin–Milwaukee (UWM). The CO_2 bubbling method was performed with the application of ultrasonication to introduce homogeneous Gr into the Mg matrix (AZ91). Graphene peaks have been successfully identified by Raman Spectroscopy and X-ray diffraction (XRD) on the precipitated carbon by dissolving Mg/Gr composite into diluted H_2SO_4. This approach also demonstrates a significant enhancement in the mechanical properties of AZ91/Gr composite.

Keywords: metal matrix composites (MMCs), in-situ Gr, graphene, magnesium AZ91, mechanical and structural properties, CO_2

INTRODUCTION

In today's world, many researchers have increasingly dealt with developing new environmentally friendly and enhanced materials used in widespread applications such as aerospace,[1] automotive,[2] and medical.[3] Lightweight materials such as Al,[4–6] Mg,[7,8] and Ti[9] are interesting candidates that can be used in the aforementioned applications. In fact, Mg has attracted a great deal of research attention on account of its low density (one-fifth of steel and 35% lighter than Aluminum),[2,10] 100% recyclability,[11,12] high specific strength,[13] and biocompatibility.[14] However, insufficient absolute strength and ductility of magnesium because of its HCP structure as well as poor creep, corrosion resistance and tribological properties are the barriers for use in high-tech applications. Consequently, researchers have been trying to enhance the mechanical and structural properties of Mg and its alloys by incorporating of hard materials such as ceramic particles,[15] whiskers,[16] nanotubes and wires.[17] Graphene has outstanding properties and has shown promise in manufacturing advanced materials. Graphene is a freestanding layer of graphite with a thickness of one atom (0.34nm), making it the first 2D material produced by humans.[18] The unique mechanical and structural properties of Gr are shown in Table 1. These properties improve with an increase in the degree of crystallinity and quality of Gr, characterized by a tightly packed and dewrinkled structure.[19] Broadly speaking, two main types of Gr defects can form in the Gr structure: vacancies and edges.[20] Monovacancy, bivacancy, and trivacancy are three observed vacancies in Gr sheets.

Recently, many researchers have conducted investigations to synthesize and subsequently homogenously disperse in-situ Gr into molten magnesium by conducting different routes, e.g., bubbling CO_2 gas,[21] direct injection of polymer precursor,[22] adding ex-situ Gr particles,[23] and the Covetic method.[21] Figure 1 illustrates a schematic of the mechanism that occurs during the reaction between CO_2 gas and Mg melt, resulting in in-situ formation of MgO and Gr. The mechanism of in-situ formation of Gr sheets

in the molten magnesium is discussed later in the section "CO_2 Injection into Molten Magnesium."

Table 1. Some Examples of Prominent Mechanical and Physical Properties of Gr[18,24,25]

Thermal conductivity	1500 $cm^2 V^{-1}S^{-1}$
Resistivity	$10^{-6}\Omega$-cm
Elastic modulus	0.5 – 1 TPa
Coefficient of thermal expansion	-6×10^{-4} /K
Specific surface area	2630 m^2g^{-1}
Young's modulus	1TPa
Thermal conductivity	5000 W/mK
Electron mobility	250000 $cm^2/(Vs)$
Tensile strength	130 GPa

According to the rule of mixtures,[26] by adding a hard phase into a soft metal matrix, an enhanced composite with tailored properties between the hard phase and the metal matrix is achieved. As a result, Gr has a great potential to increase the mechanical and physical properties of Mg alloys. The Mg/Gr composites can be used in high-tech applications such as biomedical, transport, and aerospace due to their high tribological properties, biodegradability, and non-toxicity.[27] However, owing to the nanoscale thickness of Gr sheets and high reactivity of molten magnesium, there are long-standing challenges to fabricate a homogenous Gr reinforced magnesium with a sustainable, large-scale, and reproducible method for fabricating Gr reinforced magnesium matrix composites.[23]

In this work, a sustainable, environmentally friendly and cost-effective method of introducing Gr particles within the molten AZ91 was performed. The composite fabricated by CO_2 bubbling is 40% cheaper than the corresponding composite containing the same graphene content reinforced ex-situ, with a cost of $82/lb for the AZ91 composite synthesized via CO_2 bubbling, compared to $140/lb for the AZ91 composite fabricated using ex-situ graphene embedding. A novel approach to introduce Gr with the application of a high-frequency ultrasonication was designed to facilitate the dispersion of Gr within the Mg melt.

We believe that the ultrasonic process during CO_2 bubbling would have a profound impact on Gr dispersion leading to a significant improvement in mechanical properties of AZ91/Gr composite. The scanning electron microscopy (SEM), XRD, and Raman Spectroscopy have confirmed the formation of Gr trough CO_2 bubbling. The mechanical properties of the AZ91 composite are compared to the AZ91 control sample.

THERMODYNAMICS OF GR FORMATION IN METAL SYSTEMS

There is no prior comprehensive research specifically addressing the thermodynamics of Gr formation via CO_2 bubbling in molten magnesium. However, we have collected relevant literature that explores similar reactions involving gas-metal interactions, particularly those focusing on the reactions between various gases and molten metals leading to the form of Gr/metal bonding. Xu et al.[28] used Co (0001) as a substrate for Gr growth with C_2H_4 acting as the precursor. The precursor is essentially a carbon-rich source that breaks down at high temperatures, giving rise to carbon atoms that form Gr on the substrates. It was found that the annealing of carbon-covered Co (0001) surfaces at temperatures above 580 K leads to the transformation of C_1 adatoms and C_2 dimers to Gr in an endothermic process. The calculated enthalpies for those reactions were estimated to be 261 kJ and 287 kJ, respectively.

The study showed that the reaction of C_2 to Gr has higher activation energy as compared to the C_1 to Gr reaction, but this does not lead to the formation of C_2 dimers during the C_1 to Gr reaction. The authors recommended that the calculation of the growth rate of Gr should be based on the carbon cluster attachment rate when C_1 and carbon clusters are present in the system at the same time in the form of precursors.

Wang et al.[29] studied the formation of triangular Gr flakes on a Ni (111) substrate which demonstrated a zigzag (ZZ) and ZZ-Klein edges. These initial triangular Gr islands underwent further growth leading to the formation of hexagonal Gr flakes. Gr growth on a Ni (111) surface occurs based on two, i.e., armchair (AC) or zigzag (ZZ), edges. The formation energies for different edge growth mechanisms and two different stacking methods, on top and inlay, as well as for face-centered cubic (FCC) and HCP stacking were calculated and are presented in Table 2.

Table 2. Comparison of Decrease of C1 and C2 Atoms and Growth of Gr at Varying Temperatures[28]

	Temperature	C_1 or C_2 decrease ($x10^{-6}$/h)	Graphene growth ($x10^{-6}$/h)	C_1 or C_2 decrease/ Graphene growth
C_1-to-graphene transformation reaction	610 K	4.77 0.26	7.42 0.63	0.64
	620 K	8.79 0.39	12.53 0.53	0.70
	625 K	10.16 0.53	14.79 0.68	0.69
	630 K	12.32 0.53	17.79 0.53	0.69
C_2-to-graphene transformation reaction	615 K	1.58 0.14	2.48 0.14	0.64
	620 K	3.35 0.19	4.44 0.19	0.75
	625 K	4.77 0.31	6.91 0.47	0.69
	630 K	6.60 0.47	9.42 0.47	0.70

It was observed that the formation energies for the FCC stacking were lower than those of HCP for every edge growth mechanism. The Gr nano islands were found to be formed on by the ZZ edge with FCC stacking for both on-top and inlay modes. It was concluded that in a thermoequlibrium condition a hexagonal or truncated triangle is possible but if the kinetics of Gr growth are controlled, triangular islands are formed.
The growth of epitaxial Gr on the Si side of a 3C-SiC (111) substrate was found to be in the form of thermodynamically stable phases. The process implemented the sublimation of Si from the SiC substrate in order to promote the bonding of carbon atoms to form Gr. The study found that control of the pressure and temperature conditions affects the Gr growth on SiC. The equilibrium conditions for the surface phases were represented by Eqn. 1:

$$\gamma_{Si-face} + \gamma_{C-face} = \frac{1}{A}\left(E^{slab} - N_{Si}\mu_{Si} - N_C\mu_C\right) \quad \textbf{Eqn. 1}$$

Where: μ_{Si} and μ_C are the chemical potentials and N_{Si} and N_C are the number of atoms of Si and C. The γ_{Si} and γ_C are the surface energies of Si and C, A is the area, and E^{slab} is the total energy of the geometry.[30]

The growth of Gr on the Cu surface during chemical vapor deposition (CVD) process takes place on account of dehydrogenation process.[31] The gas precursor, which is hydrocarbon gas undergoes decomposition leading to carbon atoms forming Gr layers. The dehydrogenation on a Cu (111) surface was found to be an endothermic process with activation energy barriers in the range of 1.0 eV to 2.0 eV. Equation. 2 was presented to calculate the chemical potential of carbon at a growth temperature of 1300 K and a chemical equilibrium between CH_4 and H_2 in gas phase.[32]

$$\mu_C = -2\mu_H - 10.152 + 0.112\ ln\chi \quad \textbf{Eqn. 2}$$

Where: μ_C and μ_H are the chemical potentials of carbon and hydrogen and χ is the ratio of partial pressure of carbon and hydrogen. Kim, et al.[33] defined an equation for calculating the growth of Gr as shown in Eqn. 3:

$$A_G = 1 - \frac{(p_{H_2})^2}{K_1K_2K_3\rho_S P_{CH_4}} \quad \textbf{Eqn. 3}$$

Where: ρ_s is the density of surface sites on Cu surface, K_1 is the adsorption and desorption equilibrium of CH_4 decomposition reaction, K_2 is the adsorption and desorption of H_2, and K_3 is the attachment and detachment of carbon atoms on edges of Gr islands.

Losurdo et al. studied the growth of Gr on copper and nickel substrates using CH_4-H_2 gaseous precursors and the involvement of hydrogen in the kinetics and structure of Gr formation. The kinetic characterization was performed using a non-destructive and non-intrusive spectroscopic ellipsometry, which works by measuring the pseudo dielectric function of the Gr layers. The Gr was further characterized by Raman spectroscopy. The Gr growth kinetics on Cu and Ni surfaces is affected by the H_2 which has an affinity to diffuse in Cu as opposed to the recombination process on the Ni surface. This H_2 acts as the kinetic inhibitor to allow for the growth of Gr on the Cu surfaces. In the case of Ni substrate, the resurface and surface combination allow to keep the Ni substrate dehydrogenated which leads to the diffusion and segregation of carbon on the Ni surface as seen in Figure 2.[34]

Table 3. Formation Energies for Zigzag (ZZ) and Armchair (AC) Edges on a Ni (111) Substrate with Different Stacking and Growth Mode (eV/nm)[29]

Edge type / Stacking		ZZ	ZZ-Klein	AC	AC-Klein
On-top	fcc	3.40	4.11	5.90	4.93
	hcp	3.73	4.46	6.27	5.40
Inlay	fcc	2.99	2.99	3.74	4.04
	hcp	3.69	7.06	5.05	5.99

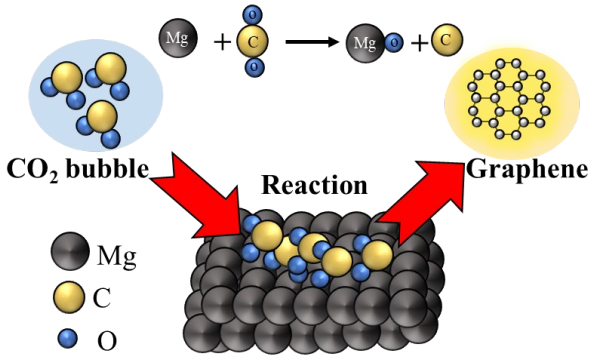

Figure 1. A schematic of in-situ Gr formation into the molten metal.[21]

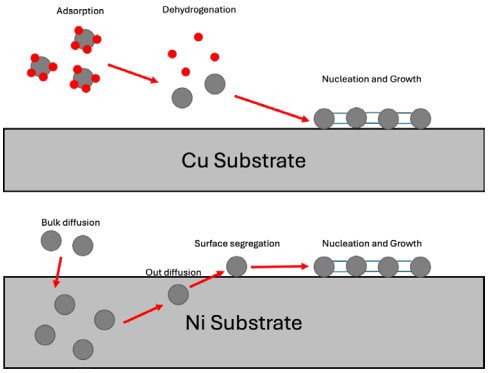

Figure 2. Gr formation in the case of Cu substrate on account if chemisorption/deposition (steps 1-3) and Ni substrate by precipitation/segregation (steps 4-6).[34]

Hao et al. [35] reported that presence of O leads to a decrease in the nucleation density of Gr. It also led to a decreased coverage of the film of Gr on the Cu substrate due to decrease in nucleation density. The second effect of O presence on the Cu substrate also causes the formation of larger Gr single-crystals. This is experimentally verified by the use of oxygen rich (OR) and oxygen free (OF) Cu substrates and growing single crystal Gr on the substrates as shown in Figure 3.

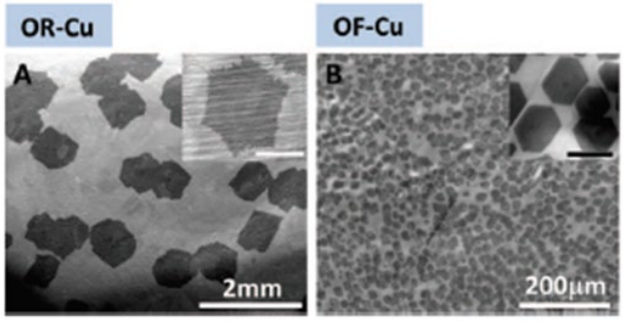

Figure 3. Comparison of Gr morphologies grown on an oxygen rich (OR) Cu substrate (A) and an oxygen free (OF) Cu substrate. The OR Cu substrate confirms the absence of a high number of nucleation sites and larger grains whereas the OF Cu substrate has much finer grains and higher number of nucleation sites.[35]

The presence of O leads to reduction of energy barrier required for edge attachment. This facilitates the nucleation and growth of Gr on the substrate. Li et al.[36] found that growth of Gr during the CVD process is governed by adsorption, diffusion, dissociation, dehydrogenation, and lattice attachment steps.[36] Celebi et al. [37] studied the growth kinetics of Gr on a Cu substrate using the Gompertz sigmoidal function. The experimental study of CVD growth on Cu substrate presented the following equation (Eqn. 4) based on the Gompertz function which defines the area of the Gr flake:

$$A(t) = A_{max} \exp\left\{-\exp\left[-\frac{\mu_m e}{A_{max}}(t-\lambda)+1\right]\right\} \quad \textbf{Eqn. 4}$$

Where, A(t) is the Gr flake area (μm^2), A_{max} is the maximum flake area (μm^2), μ_m is the maximum growth rate and λ is the time lag (min).

McCarty et al. [38] experimented with segregation of carbon and growth of Gr on Ru (0001) bulk surface during cooling. By measuring the reflectivity of the C adatoms on the Ru (0001) surface it was seen that as the temperature decreased from 1046 to 846C (1915 to 1555F) to , the concentration of C adatoms increased on the surface. It was observed that below 800C (1472F), the

concentration of C adatoms decreased as the Gr nucleation began.

Segregation of C atoms from the bulk material was driven by the Langmuir-McLean model[39] given by Eqn. 5:

$$\frac{c_s^{eq,b}}{1-c_s^{eq,b}} = \frac{c_b}{1-c_b} e^{-\Delta G_{seg}/kT} \quad \textbf{Eqn. 5}$$

Another study conducted by Zarotti et al.[40] observed the evolution of Gr on 3C SiC (111)/Si(111) substrate as a function of annealing temperature. They characterized the Gr growth mechanism on the basis of Eqns. 6 & 7:

$$SiC \longrightarrow (Si)_v + C^* \quad \textbf{Eqn. 6}$$

$$C^* + G_n \longrightarrow G_{n+1} \quad \textbf{Eqn. 7}$$

Sublimation of Si atoms during the process leads to formation of 2D Gr hexagonal structure from the carbon atoms in a bottom-up Gr growth mechanism. This movement of Si atoms is defined by Fick's first law that is modified to the Eqn. 8 form with D_{Si} being the diffusion coefficient of silicon and c_i is the concentration of the mobile silicon:

$$J_{Si} = D_{Si} \frac{c_i}{h} \quad \textbf{Eqn. 8}$$

Another study led by Wu et al.[41] found that Gr growth can be performed by an atom exchange process that occurs due to carbon atom penetration. It was found that adsorption of a carbon atom on to a bridge sire essentially caused the penetration of the carbon atom on interfacial Cu in an exothermic reaction. This happens due to overcoming the energy barrier of the process and the thermodynamic driving force leads to the movement of carbon adatoms from the Gr to Cu surfaces. Such carbon atoms start forming clusters which then leads to the nucleation process.

Li et. al. [42] have described the Gr growth using Eqn. 9 that describes the adsorption rate of gas molecules, i.e., the precursor gas. The equation brings into factor the mass that is impinging on the plane (m_i), the area (A), the temperature (T), and the pressure (P_i).

$$r_i^{ad}(T, P_i) = S_i(T) \frac{P_i A}{\sqrt{2\pi m_i k_B T}} \quad \textbf{Eqn. 9}$$

which depends on the partition functions and dissociative adsorption barrier E_a, is defined as the sticking coefficient which essentially defines the probability with which the collision of the gas molecules will adhere to the substrate thus promoting the growth of Gr on account of adsorption (Eqn. 10).

$$S_i(T) = \frac{q_{TS,i}^{vib}}{q_{gas,i}^{trans,2D} q_{gas,i}^{vib} q_{gas,i}^{rot}} exp\left(-\frac{E_a}{k_B T}\right) \quad \textbf{Eqn. 10}$$

Amini [43] developed an experimental method for growth of large area Gr in metal-carbon melts. This is a crucial technique as the application of metal-Gr composites is finding use in a variety of industries on account of its improved mechanical and tribological properties while maintaining a light weight. The growth rate of the Gr was defined by the use of undercooling (ΔT) or supersaturation (ΔC) as the growth driving force. Figure 4 shows that formation of graphitic flakes requires a smaller undercooling as well as a lower driving force as compared to the formation of the graphite spheres. Another aspect discussed is the effect of impurities on the growth kinetics.

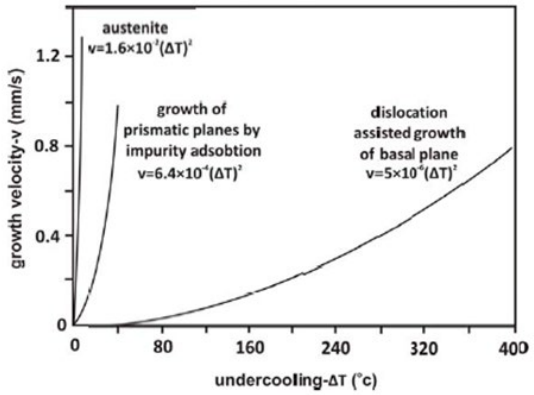

Figure 4. Growth rates of austenite and graphite prismatic planes as well as dislocation assisted growth rate of basal plane.[43]

It can be observed from Figure 5 that the presence of impurities in the metal melt can lead to lower free energy of nucleation and, thus, help to reduce the required undercooling for the Gr growth.

An aspect to be understood from this study is the possible application of the Gr growth towards forming Gr in a metal melt. A hypothetical experiment can be considered wherein Ni micro flakes are introduced into an Al melt. The Ni micro flakes are saturated with excess carbon to promote the diffusion of carbon onto the flake surface leading to Gr growth. By understanding the thermodynamics of Gr formation in such a scenario of Ni micro flakes being surrounded by Al melt, a composite can be synthesized with an Al matrix reinforced with Gr coated Ni micro flakes. As the density of Ni is higher than that of Al, it will not float much like Gr, and the higher wettability of Ni will help to form an improved bonding between Gr and the Al matrix. Such a hypothetical composite will exhibit improved tribological properties on

account of Gr formation, improved mechanical properties, and possibly lower density. A similar mechanism can be assumed for Cu micro flakes.

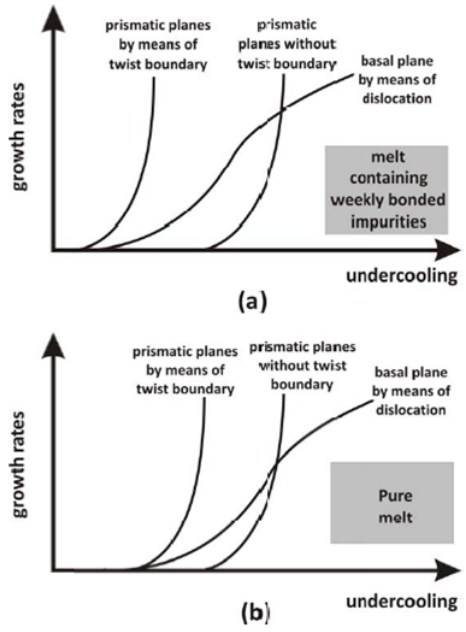

Figure 5. The comparison of a metal melt containing impurities as opposed to a pure metal melt.[43]

STRENGTHENING MECHANISMS IN GR REINFORCED MG MATRIX COMPOSITES

In Gr-reinforced magnesium (Mg) matrix composites, several strengthening mechanisms come into play to enhance the overall mechanical properties of the material, which will be addressed in this section. These mechanisms include:

1. LOAD TRANSFER MECHANISM

Gr has an exceptionally high tensile strength and stiffness. When embedded within the Mg matrix, Gr can efficiently transfer the applied load from the weaker matrix to the stronger Gr reinforcement. This results in improved overall strength and stiffness of the composite. In the work by Rashad et al.,[44] Mg-Al-Gr composites are synthesized using a semi-powder metallurgical method followed by hot extrusion. They have shown that the load transfer mechanism plays a crucial role in enhancing the material's strength. The Gr nanoplatelets (GNPs) act as reinforcements, allowing efficient load transfer from the Mg matrix to the reinforcement phase. This transfer is facilitated by the strong interfacial bonding between the GNPs and the Mg matrix, which is confirmed through X-ray mapping showing a uniform distribution of GNPs within the matrix. When external stress is applied, the load is transferred from the relatively softer Mg matrix to the stiffer GNPs, which have high elastic modulus values. This load transfer mechanism significantly contributes to improving the composite's yield strength. Theoretical models, such as the shear lag model, are used to describe this load transfer, where the reinforcement phase bears more of the applied stress, enhancing the overall mechanical properties of the composite. Similar results are shown in the work by Goh et. al,[45] where carbon nanotubes are dispersed in Mg. Another research work by Du et al.,[23] shows theoretically that the load transfer of GNPs contributed to a 72% strength improvement in a Mg alloy(ZK60)/GNP composite produced by melt stirring and hot extrusion processes. The load transfer mechanism is a key contributor to the simultaneous improvement in strength and ductility of the composites.

2. OROWAN STRENGTHENING

This mechanism arises when the Gr sheets act as obstacles to the movement of dislocations within the Mg matrix. The dislocations are forced to bypass the Gr sheets, which requires additional energy, effectively increasing the yield strength of the composite. The smaller the Gr particles, the more effective this mechanism becomes. In another paper by Rashad et al.,[46] they have shown the effectiveness of Gr in impeding the dislocation motion in pure Al-Gr composites, prepared from a semi powder methos followed by hot extrusion. They have shown that the addition of 0.3% GNPs shows an improvement in yield strength (+14.7%), UTS (+11.1%), lower failure strain (-40.6%) and higher Vickers hardness (+11.8%). Similar results are shown in a Cu-Gr composite by Chen et al.,[47] where Cu/GNPs composites of various concentrations were prepared (0.2, 0.4, 0.6, 0.8, 2.0 and 4.0 vol%) by using a wet sol-gel process and sintering. Yield strength increased with GNP content until 0.6 vol% (from 142 MPa to 310 MPa) and then decreased with further Gr additions (to 200 MPa at 4.0 vol%). Parallels can be drawn from their conclusions that similar mechanisms would contribute to the enhancement of strength in Magnesium based composites as well.

3. GRAIN REFINEMENT

The presence of Gr can inhibit grain growth during solidification or processing of the Mg matrix composite. Smaller grain sizes lead to an increase in strength due to the Hall-Petch relationship. According to this relationship, grain boundaries act as barriers to dislocation movement. As the grain size decreases, the number of grain boundaries increases, making it more difficult for dislocations to move through the material. This resistance to dislocation motion enhances the material's strength, a phenomenon known as grain boundary strengthening. Thus, reducing grain size generally results in a stronger material. In the work by Xiong et al.,[48] GNP/Al

composites are prepared by high energy ball milling and spark plasma sintering. They composites prepared at 600C showed an improvement in yield strength from 68 to 123 MPa between Pure Al and Al/GNPs. Among other strengthening mechanisms discussed in their work (such as orowan strengthening, solid solution strengthening, coefficient of theral expansion CTE) mismatch and load transfer mechanism), the effect of grain refinement has also been shown although the specific contribution of grain refinement has not been calculated.

4. THERMAL MISMATCH AND CTE

There is a mismatch in the coefficient of thermal expansion between Gr and Magnesium. This mismatch creates residual stresses at the matrix-reinforcement interface during cooling, which can inhibit dislocation movement and increase the strength of the composite. The paper by Xiong et al, has shown a calculated $\Delta\sigma_{CTE}$ to be 20.20 MP in Al/GNPs, which is lightly higher than the composite free of interfacial reaction. The CTE of GNPs, and Al is 1.0 x 10^{-6} /K and 23.6 x 10^{-6} /K, , respectively. Similar mechanisms can be expected in Mg/Gr composites as the CTE for pure magnesium is 25.2 x 10^{-6} /K , which is slightly higher than that of Al between 20-100˚C (36-180˚F).

5. DISPERSION STRENGTHENING

Uniform dispersion of Gr within the Mg matrix leads to strengthening by impeding the motion of dislocations. This phenomenon is similar to how other second-phase particles strengthen a metal matrix, where dispersed Gr flakes act as barriers to dislocation glide, enhancing the yield strength and hardness of the composite. In the review by Baig et al.,[49] the authors highlight dispersion strengthening as one of the key factors for enhancing the mechanical properties of metal matrix nanocomposites reinforced with carbon nanofillers like Gr and carbon nanotubes. They discuss how uniform dispersion of nanofillers is critical for realizing the full potential of their strengthening effects. Proper dispersion helps in preventing the agglomeration of nanoparticles, which can otherwise lead to defects like cracks or voids in the matrix, reducing the mechanical performance of the composite. When well-dispersed, the nanofillers effectively block dislocation motion and contribute to other strengthening mechanisms like load transfer and Orowan strengthening. Achieving homogeneous dispersion early in the powder mixing process is crucial and different techniques such as mechanical alloying, colloidal processing, and hybrid methods could be useful to optimize dispersion and ensure the nanofillers are uniformly distributed throughout the matrix.

6. INTERFACIAL BONDING

Strong interfacial bonding between Gr and the metal matrix contributes to improved mechanical properties. Good bonding ensures efficient load transfer between the Gr reinforcement and the matrix, as well as enhancing resistance to crack initiation and propagation. The paper by Shi et al,[50] discusses the effect of Gr on interfacial bonding in copper MMCs by highlighting how Gr nanoplatelets (GNPs) improve the interface between the reinforcement and the metal matrix. The strong in-plane bonding of Gr, due to its sp^2 hybridized carbon structure, allows for enhanced load transfer and prevents crack initiation at the interface. Moreover, Gr's large surface area promotes better interaction and mechanical interlocking with the metal matrix, further strengthening the composite through effective stress distribution. Jing et al.,[7] have shown that the strong interface bonding between Gr and the substrate through MgO improves not only the thermal conductivity (74.8 W/(m·K)) but also the synergistic improvement of mechanical properties (243.1 MPa, 93.7 HV) in a composite of AZ91D alloy with 0.3 wt% GNPs.

Each of these mechanisms contributes to the overall enhancement of the mechanical performance of Mg-Gr composites, such as improved tensile strength, yield strength and hardness, while maintaining lightweight characteristics.

CO_2 INJECTION INTO MOLTEN MAGNESIUM

Equations 11 & 12 show a two-step reaction simultaneously occurs between CO_2 and magnesium[51] when CO_2 gas is introduced to the molten magnesium.[52,53] Overall, the simplified form of the in-situ reaction between CO_2 gas and magnesium is Eqn. 13 with the standard reaction Gibbs free energy Eqn. 14. One of the products of the Eqn. 13 is solid-state free carbon. Due to the low wettability and solubility of carbon atoms in the magnesium melt, these free carbon atoms preferentially tend to contact each other and form 2D Gr sheets.

$$Mg + CO_2 = MgO + CO \quad \textbf{Eqn. 11}$$

$$Mg + CO = MgO + C \quad \textbf{Eqn. 12}$$

$$Mg\ (l)+CO_2\ (g)=MgO(s)+C\ (s) \quad \textbf{Eqn. 13}$$

$$\Delta G_T^{\Theta}=3.56TlnT-17.63\times10^{-3}T^2+1.63\times10^5T^{-1}+4.92\times10^{-6}T^3+274.83T-827100.17 \quad \textbf{Eqn. 14}$$

MATERIALS AND EXPERIMENTAL DETAILS

Magnesium alloy (AZ91), highly pure CO_2 gas, and pure zinc are used as raw materials. Magnesium AZ91 (500g) was melted in a silicon carbide crucible with a Refcobar refractory coating (Refcotec, Inc.) in an electrical

resistance furnace at 800C (1472F) under a highly pure argon atmosphere to prevent burning. Once melted, the molten magnesium underwent ultrasonication at 1800 KHz. Meanwhile, CO_2 was introduced into the molten Mg at a flow rate of 7 $L.min^{-1}$ using a stainless-steel exhaust muffler for 10 minutes. Highly pure zinc was added during the process to enhance the reaction efficiency. The slurry was then poured into a permanent mold. Another sample with the same conditions without CO_2 injection was fabricated as the control sample. Figure. 6 shows the experimental setup used for the fabrication of AZ91/Gr composite.

Electron microscopy, Raman spectroscopy, Vickers hardness tests with a 1000g load, and tensile tests were performed to investigate the morphology of the Gr and the mechanical properties of the final sample. To measure the tensile strength, dogbone-shaped specimens were machined according to the ASTM EM8 with a gauge length of 30 mm and 6 mm diameter.

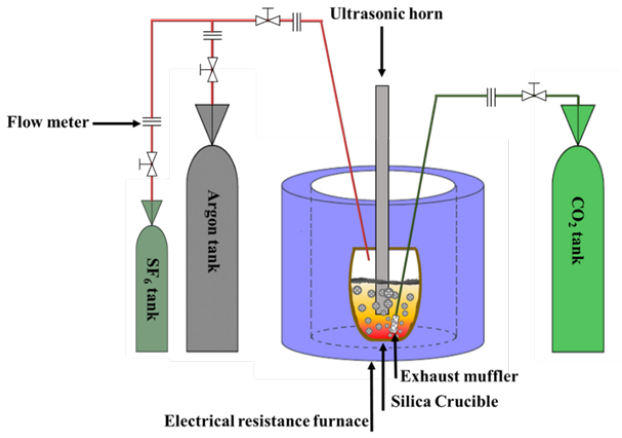

Figure 6. Schematic of the CO2 bubbling set up.

RESULTS AND DISCUSSION

The reaction steps between CO_2 and Mg are shown in Figure 7. The first stage involves the injection of CO_2 gas into the molten magnesium. According to the buoyant law, when a bubble is introduced into the molten metal, it strives to reach the surface as quickly as possible. Additionally, due to the relatively low height of the Mg melt, the bubbles reach the surface rapidly. When the CO_2 bubbles encounter the high-temperature molten metal, they experience a sharp expansion in accordance with the ideal gas law. This expansion increases the surface contact between the bubbles and the molten magnesium. In this stage, CO_2 molecules on the surface of the bubbles begin to react with magnesium atoms, resulting in a reduction reaction (Eqns. 11-14). Consequently, the concentration of carbon on the gas/liquid interface gradually increases. Once a certain carbon concentration is reached on the inner surface layer, Gr nucleation occurs(step 2).

Step 3 represents Gr nuclei becoming more stable and bigger in this stage. The predominant Gr sheets on the inner surface of the bubbles start growing. The growing rate of the Gr sheets depends on the concentration and purity of the CO_2 gas. It is readily apparent that increasing the duration of sustainability of bubbles in the molten magnesium would result in bigger Gr sheets. This can provoke the sustainability of Gr sheets in molten metals. Step 4 is the final and most important stage.

Ultrasonication causes the shattering of the expanded CO_2 bobbles into smaller ones. This phenomenon is the key for Gr dispersion into the molten metal. Besides this, ultrasonication breaks agglomeration into smaller parts in case of agglomeration.

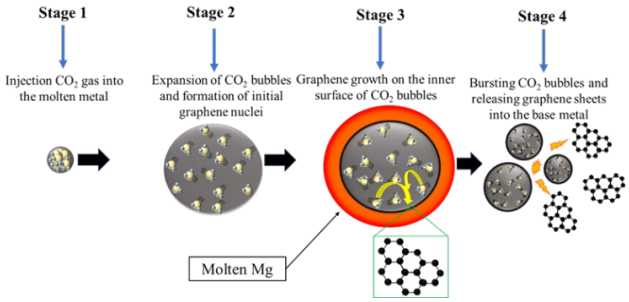

Figure 7. Graphene formation steps in magnesium medium.

Figure 8 shows the microstructure evolution in two magnifications before (a&c) and after (b&d) the gas treatment. The microstructure comprises two phases, α and β. Both α and β phases of the composite sample are smaller than the control sample. Once the Gr forms in Mg melt, it acts as nucleation sites, leading to a reduction in grain size and enhancing the mechanical properties. After solidification, the Gr particles also play a crucial role in pinning and making barriers against dislocation movements.

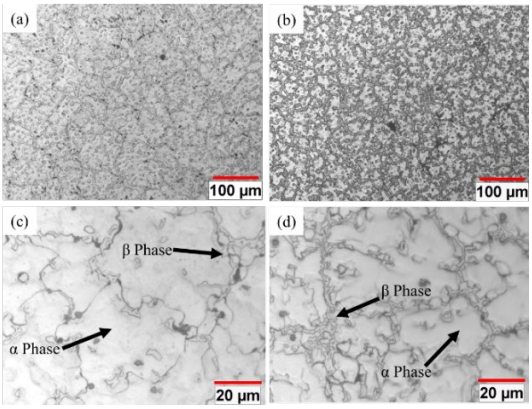

Figure 8. Microstructural evolution after and before CO_2 bubbling in two different magnifications.

Figure 9 illustrates the Raman spectroscopy of the composite and control samples. The composite sample exhibits peaks at 1350 cm^{-1}, 1590 cm^{-1}, and 2700 cm^{-1}, which correspond to the D, G, and 2D bands, respectively. The presence of these peaks indicates the successful formation of Gr within the molten metal. Figure 10 shows SEM of the surface of the sample with elemental mapping. It shows some areas enriched with carbon atoms that represent the presence of a carbon phase produced by CO_2 bubbling. Based on the Raman spectroscopy result, these areas would be agglomerations of Gr in the AZ91 matrix. Zn was not detected in either control or composite samples and it evaporated during the casting process. According to Luchetta et al.'s findings, Zn vapor enhances graphene porosity and improves CO_2 interaction with Mg, which results in a higher yield of graphene.[54]

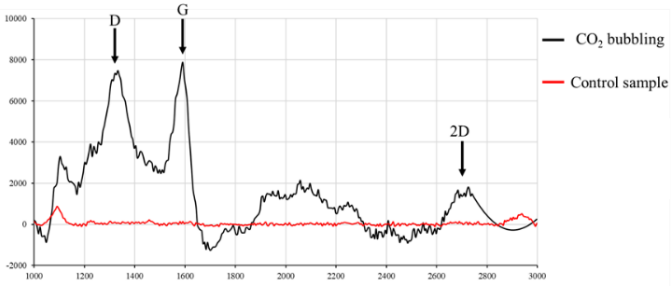

Figure 9. Raman spectroscopy from control and Mg-Gr composite.

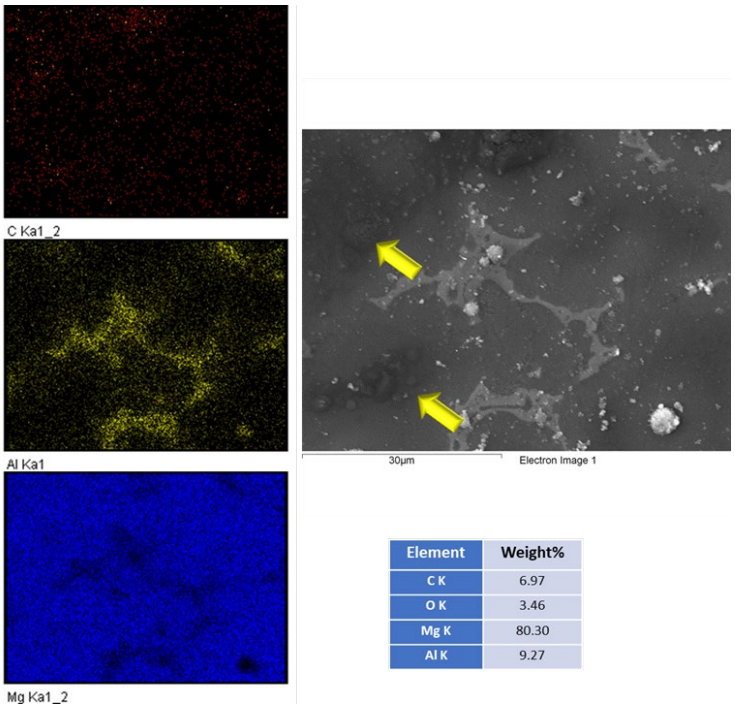

Element	Weight%
C K	6.97
O K	3.46
Mg K	80.30
Al K	9.27

Figure 10. SEM and elemental mapping of the composite sample.

A dilute H_2SO_4 solution (2 $mol.L^{-1}$) was adopted to remove the MgO, residual Mg and Zn by immersing the bulk composite at room temperature. The mixture was then filtered and washed with deionized water 5 times and dried in the oven. The resulting powder was collected for further SEM investigation. Figure 11 shows the SEM image with the corresponding elements mapping image. Based on the mapping analysis, it is readily apparent that the collected powder has a considerable amount of carbon. This result demonstrates the successful in-situ synthesis of Gr flakes in molten magnesium. Figure 12 shows XRD pattern obtained from the residues of dissolving Gr/Mg composite in acid. A small peak at $2\theta = 25.8^\circ$ is proof of the formation of Gr in the Mg matrix.

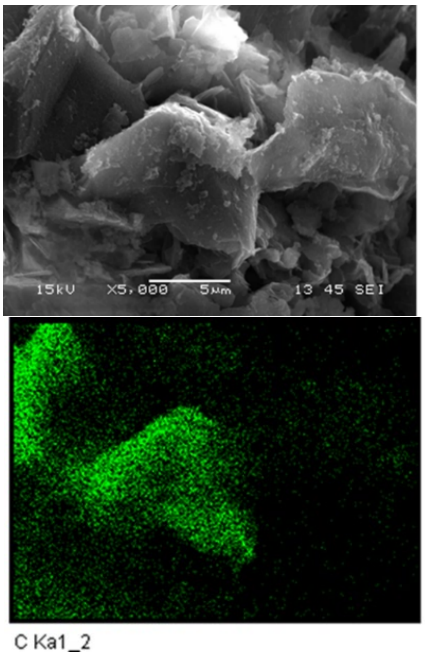

Figure 11. Elemental mapping of the extracted powder from the composite sample.

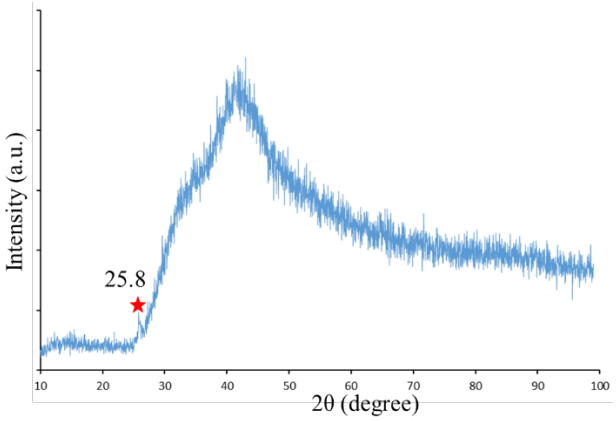

Figure 12. The XRD pattern of the dissolved Gr/Mg composite.

The Vickers hardness of the composite sample is 16.5% higher than the control sample (Figure 13). The tensile test also shows a 20% enhancement in fracture strength of the composite sample compared to the control sample. Mechanical improvement can be attributed to the strengthening mechanisms and load transfer mechanism resulting from the presence of Gr particles within the matrix. Moreover, the improved strength of the composite sample indicates the successful synthesis of Gr particles through CO_2 injection.

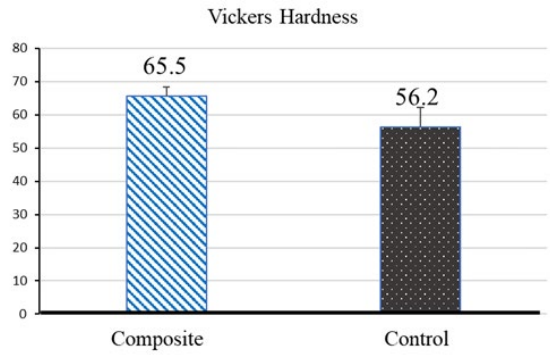

Figure 13. Vickers hardness of composite and control samples.

CONCLUSION

This paper consists of two main parts. First, a review of the recently published literature on the synthesis of in-situ Gr/Mg matrix composites was presented. Second, the results of the experiments conducted at UWM were discussed. In the latter, Gr/Mg matrix composites were synthesized using a scalable and environmentally-friendly route, i.e., simultaneous ultrasonication and CO_2 gas bubbling of the AZ91 melt to introduce Gr particles within the AZ91 matrix.

The main conclusions of the paper are as follows.

- CO_2 bubbling is a reliable method for synthesizing Gr/Mg composite with an acceptable Gr formation efficiency.
- The precipitation of Gr has been studied across multiple metal systems using carbon-based precursors. Adsorption, absorption, sublimation, and atom exchange process are some of the successful methods in forming Gr.
- By simultaneous ultrasonication and CO_2 gas bubbling into the AZ91 melt, Gr particles were successfully synthesized and dispersed in the AZ91 matrix as confirmed by SEM, XRD and Raman spectroscopy analyses.
- Synthesis of Gr in the melt with CO_2 bubbling comprised four stages: bubble expansion, Gr nucleation, growth, and dispersion into the melt.
- The presence of Gr in melt results in improved mechanical and structural properties.

REFERENCES

1. Das, D. K., Sarkar, J., Bengal, W., et al., "Graphene Magnesium Nanocomposite: An Advanced Material for Aerospace Application," V. 1850075, 2018, pp. 1-8.
2. Cevik, E., and Gundogan, M., "Dry Sliding Wear Behavior of (GNPs + TiB2)-Reinforced AZ91 Magnesium Matrix Hybrid Composites Produced by Pressure Infiltration Casting Method," *International Journal of Metalcasting*, V. 15, No. 4, 2021, pp. 1250–9.
3. Rashad, M., Pan, F., Asif, M., et al., "Corrosion behavior of magnesium-graphene composites in sodium chloride solutions," *Journal of Magnesium and Alloys*, V. 5, No. 3, 2017, pp. 271–6.
4. Zare, M., Maleki, A., and Niroumand, B. "In situ Al-SiOC composite fabricated by in situ pyrolysis of a silicone polymer gel in aluminum melt," *International Journal of Metalcasting*, V. 16, No. 3, 2022, pp. 1327–46.
5. Moshrefifar, M., and Zare, M. "Effect of nano Si3N4 ، Al2O3 و AlMg and cold rolling process on the microstructural and mechanical properties of AL-6061alloy," *Journal of New Materials*, V. 10, No. 35, 2019, pp. 115–28.
6. Ghaderi, O., Zare, M., and Niroumand, B., Church, B. C., and Rohatgi, P. K. "Selected challenges in solidification processing of graphene nanoplatelets (GNPs) reinforced aluminum alloys composites," *Frontiers*|, V. 11, 2024, p. 1363270.
7. Jing, J., Chen, L., Li, Z., et al., "Interfacial bonding mechanism of graphene nanoplatelets reinforced AZ91D magnesium alloy prepared by semi-solid injection molding," *Journal of Alloys and Compounds*, V. 1006, 2024, p. 176171.
8. Aghayani, M. K., and Niroumand, B. "Effects of ultrasonic treatment on microstructure and tensile strength of AZ91 magnesium alloy," *Journal of Alloys and Compounds*, V. 509, No. 1, 2011, pp. 114–22.
9. Mu, X. N., Zhang, H. M., Cai, H. N., et al., "Microstructure evolution and superior tensile properties of low content graphene nanoplatelets reinforced pure Ti matrix composites," *Materials Science and Engineering: A*, V.687, 2017, pp.164-74.
10. Ye, H. Z., and Liu, X. Y. "Review of recent studies in magnesium matrix composites," *Journal of Materials Science*, V. 39, No. 20, 2004, pp. 6153–71.
11. Mindivan, H., Efe, A., Kosatepe, A. H., et al., "Fabrication and characterization of carbon nanotube reinforced magnesium matrix composites," *Applied Surface Science*, V. 318, 2014, pp. 234–43.
12. A. Javaid, E. Essadiqi, S. Bell, B. D. "Literature Review On Magnesium Recycling," 2006.
13. Chen, L., and Yao, Y. "Processing, microstructures, and mechanical properties of magnesium matrix composites: A review," *Acta Metallurgica Sinica (English Letters)*, V. 27, No. 5, 2014, pp. 762–74.
14. Bommala, V. K., Krishna, M. G., and Rao, C. T. "Magnesium matrix composites for biomedical applications : A review," *Journal of Magnesium and Alloys*, V. 7, No. 1, 2019, pp. 72–9.
15. Dey, A., and Pandey, K. M. "Magnesium Metal Matrix Composites - A Review," V. 42, 2015, pp. 58–67.
16. Chen, S. H., Jin, P. P., Schumacher, G., et al., "Microstructure and interface characterization of a cast Mg2B2O5 whisker reinforced AZ91D magnesium alloy composite," *Composites Science and Technology*, V. 70, No. 1, 2010, pp. 123–9.
17. Shimizu, Y., Miki, S., Soga, T., et al., "Multi-walled carbon nanotube-reinforced magnesium alloy composites," *Scripta Materialia*, V. 58, No. 4, 2008, pp. 267–70.
18. Cataldi, P. "Applied Sciences Graphene Nanoplatelets-Based Advanced Materials and Recent Progress in Sustainable Applications," 2018.
19. Tehrani, M. "Advanced Electrical Conductors: An Overview and Prospects of Metal Nanocomposite and Nanocarbon Based Conductors," *Physica Status Solidi (A) Applications and Materials Science*, V. 218, No. 8, 2021.
20. Kiciński, W., and Dyjak, S. "Transition metal impurities in carbon-based materials: Pitfalls, artifacts and deleterious effects," *Carbon*, V. 168, 2020, pp. 748–845.
21. Wei, S., Shi, H., Li, X., et al., "A green and efficient method for preparing graphene using CO2@Mg in-situ reaction and its application in high-performance lithium-ion batteries," V. 902, 2022.
22. Sudarshan., Terauds, K., Anilchandra, A. R., et al., "Polymer-derived in-situ metal matrix composites created by direct injection of a liquid polymer into molten magnesium," *Metallurgical and Materials Transactions A: Physical Metallurgy and Materials Science*, V. 45, No. 2, 2014, pp. 551–4.
23. Du, X., Du, W., Wang, Z., et al., "Ultra-high strengthening efficiency of graphene nanoplatelets reinforced magnesium matrix composites," *Materials Science and Engineering: A*, V. 711, 2018, pp. 633–42.
24. Prashantha Kumar, H. G., and Anthony Xavior, M. "Graphene reinforced metal matrix composite (GRMMC): A Review," *Procedia Engineering*, V. 97, 2014, pp. 1033–40.
25. Chen, T., & Cheung, R., "Mechanical properties of graphene," *Graphene Science Handbook: Mechanical and Chemical Properties*, 2016, pp. 3-15.
26. Jasiuk, I., Nilufar, S., Salamanca-Riba, L., et al., "Novel aluminum-carbon materials," *Technical Proceedings of the 2013 NSTI Nanotechnology*

Conference and Expo, NSTI-Nanotech 2013, V. 1, 2013, pp. 27–30.
27. Shahin, M., Munir, K., Wen, C., et al., "Acta Biomaterialia Magnesium matrix nanocomposites for orthopedic applications : A review from mechanical , corrosion , and biological perspectives," V. 96, 2019, pp. 1–19.
28. Xu, L., Jin, Y., Wu, Z., et al., "Transformation of Carbon Monomers and Dimers to Graphene Islands on Co(0001): Thermodynamics and Kinetics," *The Journal of Physical Chemistry C*, V. 117, No. 6, 2013, pp. 2952–8.
29. Wang, D., Liu, Y., Sun, D., et al., "Thermodynamics and Kinetics of Graphene Growth on Ni(111) and the Origin of Triangular Shaped Graphene Islands," *The Journal of Physical Chemistry C*, V. 122, No. 6, 2018, pp. 3334–40.
30. Nemec, L., Blum, V., Rinke, P., et al., "Thermodynamic Equilibrium Conditions of Graphene Films on SiC," *Physical Review Letters*, V. 111, No. 6, 2013, p. 065502.
31. Zhang, W., Wu, P., Li, Z., et al., "First-Principles Thermodynamics of Graphene Growth on Cu Surfaces," *The Journal of Physical Chemistry C*, V. 115, No. 36, 2011, pp. 17782–7.
32. Wu, P., Zhang, W., Li, Z., et al., "Mechanisms of Graphene Growth on Metal Surfaces: Theoretical Perspectives," *Small*, V. 10, No. 11, 2014, pp. 2136–50.
33. Kim, H., Saiz, E., Chhowalla, M., et al., "Modeling of the self-limited growth in catalytic chemical vapor deposition of graphene," *New Journal of Physics*, V. 15, No. 5, 2013, p. 053012.
34. Losurdo, M., Giangregorio, M. M., Capezzuto, P., et al., "Graphene CVD growth on copper and nickel: role of hydrogen in kinetics and structure," *Physical Chemistry Chemical Physics*, V. 13, No. 46, 2011, pp. 20836–43.
35. Hao, Y., Bharathi, M. S., Wang, L., et al., "The Role of Surface Oxygen in the Growth of Large Single-Crystal Graphene on Copper," *Science*, V. 342, No. 6159, 2013, pp. 720–3.
36. Li, X., Cai, W., Colombo, L., et al., "Evolution of Graphene Growth on Ni and Cu by Carbon Isotope Labeling," *Nano Letters*, V. 9, No. 12, 2009, pp. 4268–72.
37. Celebi, K., Cole, M.T., Choi, J.W., et al., "Evolutionary Kinetics of Graphene Formation on Copper," *Nano Letters*, V. 13, No. 3, 2013, pp. 967–74.
38. McCarty, K. F., Feibelman, P. J., Loginova, E., et al., "Kinetics and thermodynamics of carbon segregation and graphene growth on Ru (0 0 0 1)," *Carbon*, V. 47, No. 7, 2009, pp. 1806–13.
39. Blakely, J. M., and Thapliyal, H. V. "Structure and phase transitions of segregated surface layers," *Interfacial segregation*, 1977, pp. 137–74.
40. Zarotti, F., Gupta, B., Iacopi, F., et al., "Time evolution of graphene growth on SiC as a function of annealing temperature," *Carbon*, V. 98, 2016, pp. 307–12.
41. Wu, P., Zhai, X., Li, Z., et al., "Bilayer Graphene Growth via a Penetration Mechanism," *The Journal of Physical Chemistry C*, V. 118, No. 12, 2014, pp. 6201–6.
42. Li, P., and Li, Z. "Theoretical Insights into the Thermodynamics and Kinetics of Graphene Growth on Copper Surfaces," *The Journal of Physical Chemistry C*, V. 124, No. 30, 2020, pp. 16233–47.
43. Amini, S. "Synthesis of Graphene Layers from Metal-Carbon Melts: Nucleation and Growth Kinetics," University of California, Riverside, 2012.
44. Rashad, M., Pan, F., Tang, A., et al., "Improved strength and ductility of magnesium with addition of aluminum and graphene nanoplatelets (Al+ GNPs) using semi powder metallurgy method," *Journal of Industrial and engineering chemistry*, V. 23, 2015, pp. 243–50.
45. Goh, C. S., Wei, J., Lee, L. C., et al., "Simultaneous enhancement in strength and ductility by reinforcing magnesium with carbon nanotubes," *Materials Science and Engineering: A*, V. 423, Nos. 1–2, 2006, pp. 153–6.
46. Rashad, M., Pan, F., Tang, A., et al., "Effect of Graphene Nanoplatelets addition on mechanical properties of pure aluminum using a semi-powder method," *Progress in Natural Science: Materials International*, V. 24, No. 2, 2014, pp. 101–8.
47. Chen, F., Ying, J., Wang, Y., et al., "Effects of graphene content on the microstructure and properties of copper matrix composites," *Carbon*, V. 96, 2016, pp. 836–42.
48. Xiong, B., Liu, K., Yan, Q., et al., "Microstructure and mechanical properties of graphene nanoplatelets reinforced Al matrix composites fabricated by spark plasma sintering," *Journal of Alloys and Compounds*, V. 837, 2020, p. 155495.
49. Baig, Z., Mamat, O., and Mustapha, M. "Recent Progress on the Dispersion and the Strengthening Effect of Carbon Nanotubes and Graphene-Reinforced Metal Nanocomposites: A Review," *Critical Reviews in Solid State and Materials Sciences*, V. 43, No. 1, 2018, pp. 1–46.
50. Shi, L., Liu, M., Zhang, W., et al., "Interfacial Design of Graphene Nanoplate Reinforced Copper Matrix Composites for High Mechanical Performance," *JOM*, V. 74, No. 8, 2022, pp. 3082–90.
51. S.Yuasa, A.F. "Ignition and combustion of magnesium particles in carbon dioxide," *Applied Mechanics and Materials*, V. 152–154, 1994, pp. 1587–94.

52. Shiryaev, A. A., and Goldshleger, U. I. “Magnesium and Carbon Dioxide : A Rocket Propellant for Mars Missions,” V. 9, No. 2, 1993, pp. 197–203.
53. Abbud-Madrid, A., Byrne, L., Gatsonis, N. A., et al., “Combustion of magnesium with carbon dioxide and carbon monoxide at low gravity,” *Journal of Propulsion and Power*, V. 17, No. 4, 2001, p. 852–9.
54. Luchetta, C., Oliveira Munsignatti, E.C., and Pastore, H. O. “CO2 metallothermal reduction to graphene: the influence of Zn,” *Frontiers in Chemical Engineering*, V. 3, 2021, p. 707855.